ACS Energy Letters

http://pubs.acs.org/journal/aelccp

LETTER

Critical Role of Pressure for Chemo-Mechanical-Induced Stability of Sodium Metal Battery Anodes

Weimin Jiao, Murtaza Zohair, Janna Eaves-Rathert, Jayanth Ramamurthy, Andrew Harkaway, Rebecca Mort, Jacob Wheaton, Shan Jiang, Steve W. Martin, and Cary L. Pint*

Cite This: *ACS Energy Lett.* 2023, 8, 2711−2717

Read Online

ABSTRACT: In this work we demonstrate that cell pressure controls the morphology and stability of electroplated sodium metal deposits on carbon black nucleation layers in ether-based electrolytes. At pressures below 500 kPa we observe the presence of three-dimensional Na nuclei accompanied by low Coulombic efficiencies (CEs less than 98%). Conversely, at pressures between 500 and 1272 kPa we observe smooth, planar Na deposits, high CEs up to 99.9%, and stable electrochemical cycling. Through a series of tests conducted at elevated current densities and with or without rest stages, our findings elucidate the balance of important competing time scales for creep and morphology evolution under pressure and the rate of charge transfer that determines Na morphology and stability. This highlights how chemo-mechanical effects at pressure ranges relevant for battery packaging in coin and pouch cells are key factors in the design and operation of Na metal batteries.

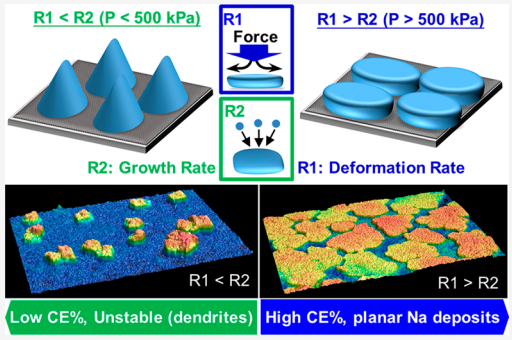

Sodium metal is one of the most promising anode options for high-energy-density and low-cost Na-based batteries. With a high theoretical specific capacity (1166 mAh g^{-1}), low standard electrode potential (−2.71 V versus standard hydrogen electrode),[1−3] and native electrochemical stability in common electrolytes, there have been a number of reports in recent years highlighting the broad promise of this system. Most notable is the anode-free battery architecture, where researchers have shown up to 400 Wh kg^{-1} active mass energy density,[4] and recent reports under lean electrolyte conditions in pouch cell architectures have demonstrated 200 Wh kg^{-1}.[5] However, other frameworks include room-temperature Na-S batteries[6−8] with a theoretical energy density of 1274 Wh kg^{-1} and Na-O_2 batteries[9−11] with a theoretical energy density of 1605 Wh kg^{-1}. Each of these systems exists in different developmental stages, but all of them exhibit improved energy density over current Li-ion batteries[1] at lower cost due to a combined 1000 times higher earth abundance of Na versus Li and lower cost and lighter options for cathode materials and current collectors, respectively.[12−14]

Early studies focused on Na metal anodes followed inspiration from Li metal anodes, with the expectation being that these two alkali metals are similar in behavior. Early observations of Na electroplating in carbonate electrolytes demonstrated behavior similar to that of Li, with unstable nucleation and growth of Na deposits accompanied by low Coulombic efficiencies (CEs, %) and dendrite formation.[15] However, researchers demonstrated that the use of ether-based electrolytes, such as diglyme, resulted in smooth crystalline electroplated Na deposits combined with CE exceeding 99.9%.[1,16] This highlights a critical difference between Na metal batteries and Li metal batteries due to the less negative reduction potential of Na that has given promise to competitive Na battery approaches.[4,5,17] In this regard, other differences between Na and Li exist, such as in mechanical and thermal properties, that have not been deeply investigated. Specifically, in regard to mechanical properties, Na is softer at room temperature than Li in metal form, with an elastic modulus of 4.6 GPa for Na and 7.82 GPa for Li.[18,19] Notably, the stress exponent for Na has been measured to be 5 versus 6.56 for Li, indicating that Na is far more susceptible to creep than Li.[18−20] Recently, by using tensile tests to measure the

Received: April 6, 2023
Accepted: May 17, 2023
Published: May 24, 2023

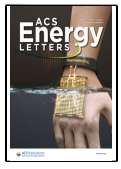

https://doi.org/10.1021/acsenergylett.3c00734
ACS Energy Lett. 2023, 8, 2711−2717

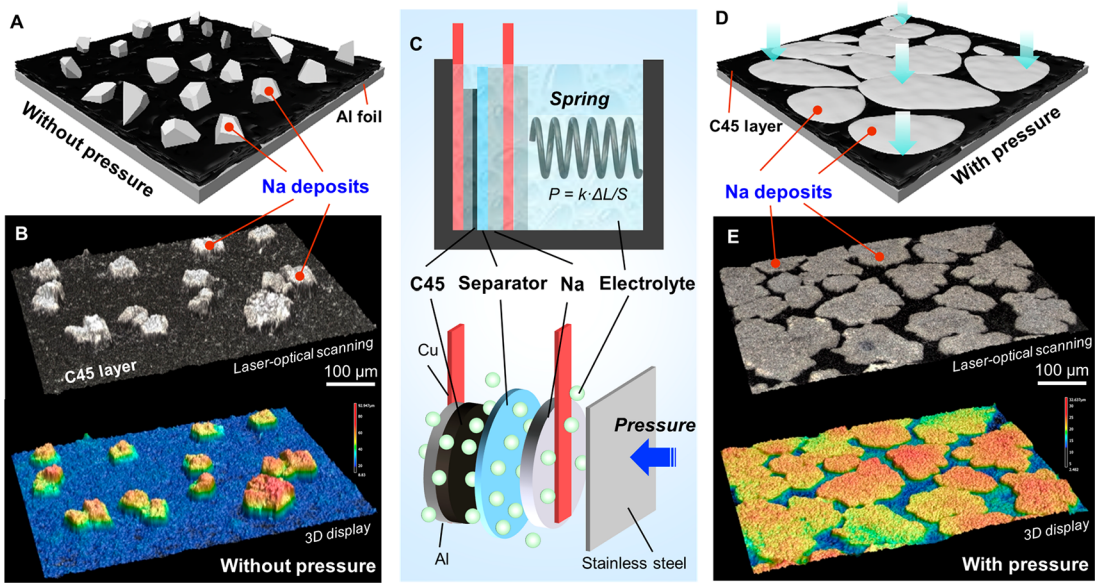

Figure 1. Impact of applied external pressure on Na electrodeposition. (A) Schematic illustration and (B) CLSM image of the Na deposits without pressure. (C) Schematic of the pressure experiment setup and the assembly configuration of the Na−thin C45 carbon black nucleation layer/Al current collector cell. (D) Schematic illustration and (E) CLSM image of the Na deposits with pressure.

temperature- and rate-dependent deformation of Na, LePage et al. reported a creep exponent value of 5.6 for Na, which implies the viscoplastic behavior of Na is expected to play a role in battery applications.[21] As creep effects do not occur in Li metal until pressures much higher than those of commercial batteries, there exists limited understanding of how the chemo-mechanical effects of Na metal impact a Na metal battery compared to those of Li in a Li metal battery.

With this said, researchers have demonstrated that applying high external pressure is a significant and effective approach to modify the chemistry and stability of Li metal deposits. Yin et al. reported a 5% improved CE during Li deposition in Li cells at 1.1 MPa pressure compared to cells with no pressure,[22] and Shen et al. ascribed these and other modifications in Li morphology to pressure effects.[23] Whereas recent advances in characterization of Li metal deposits are being studied, such as the use of Cryo-SEM,[24] a key challenge to visualizing such deposits is the air sensitivity of alkali metals. In comparison to Li, there has been limited past work on pressure effects in Na metal batteries, all of which was focused on interface properties and not morphology changes.[25,26] Therefore, given the lower yield/flow stress of Na compared to Li, which makes Na metal more sensitive to the pressure range of conventionally packaged pouch and coin cells, there is a need to better understand the pressure-induced chemo-mechanical effects in Na metal batteries.

In this report, we systematically study the effect of pressure on the nucleation, growth, and electrochemical properties of Na by combining imaging and electrochemical studies to understand the role of pressure in Na metal batteries. Our findings demonstrate that the morphology of Na deposits is highly correlated to pressure, and above pressures of 500 kPa the Na undergoes creep and/or morphology evolution that improves the electrochemical stability and reversibility of Na metal deposits. Our results explain this as a chemo-mechanical trade-off between the rate of Na charge transfer and the creep rate of Na under pressure, leading to a direct mechanical−electrochemical picture of stability in Na metal anodes.

A key motivation for this work originated from the observation that, in an *in situ* characterization cell without the external application of pressure, 3D and/or dendritic morphologies of Na were observed during Na electroplating. Comparatively, coin cells packaged under standard pressures between 500 and 1000 kPa under similar current densities led to smooth, planar morphologies of electrodeposited Na. To investigate this further, we designed a closed pressure-electrochemical cell (Figures S1 and S2) to controllably apply pressure to a Na electrode assembly consisting of 1 M $NaPF_6$ in diglyme, Celgard separator, Al/Na electrode, and Al/carbon black nucleation layer (experimental details in the Supporting Information, Figures S1, S2, and S16). A schematic of the cell and confocal laser scanning microscopy (CLSM) images showing the widely different nucleation behavior of Na over 30 min at current density 0.5 mA cm^{-2} with (1) no external pressure and (2) a pressure of 911 kPa are shown in Figure 1. With no external pressure, the formation of nuclei that protrude from the surface in a 3D growth mode (Figure 1A and B) is observed. Under uniaxial pressure (Figure 1C) of 911 kPa on the electrode assembly, smoother and lateral growth was observed for Na nuclei (Figure 1D and E). This observation elucidates that pressure plays an important role in Na nuclei morphology in a battery.

To systematically study the effect of pressure on Na metal nucleation and growth during electrodeposition, we analyzed the electrochemical and morphological behavior of Na electroplating under six different pressure conditions: 0, 22, 136, 500, 911, and 1272 kPa. It should be noted that the pressure values provided here are approximate since our experimental setup is not designed to dynamically regulate pressure; i.e., when the Na is plating, the spring will dynamically extend, and it will relax during the stripping periods. Generally, as the pressure inside of a coin cell assembly is near ∼1 MPa, this range of pressures gives detailed resolution of the effects on electroplating between no applied pressure and pressures practical to battery packaging. To study the effect of pressure on the cells, we carried out galvanostatic

https://doi.org/10.1021/acsenergylett.3c00734
ACS Energy Lett. 2023, 8, 2711−2717

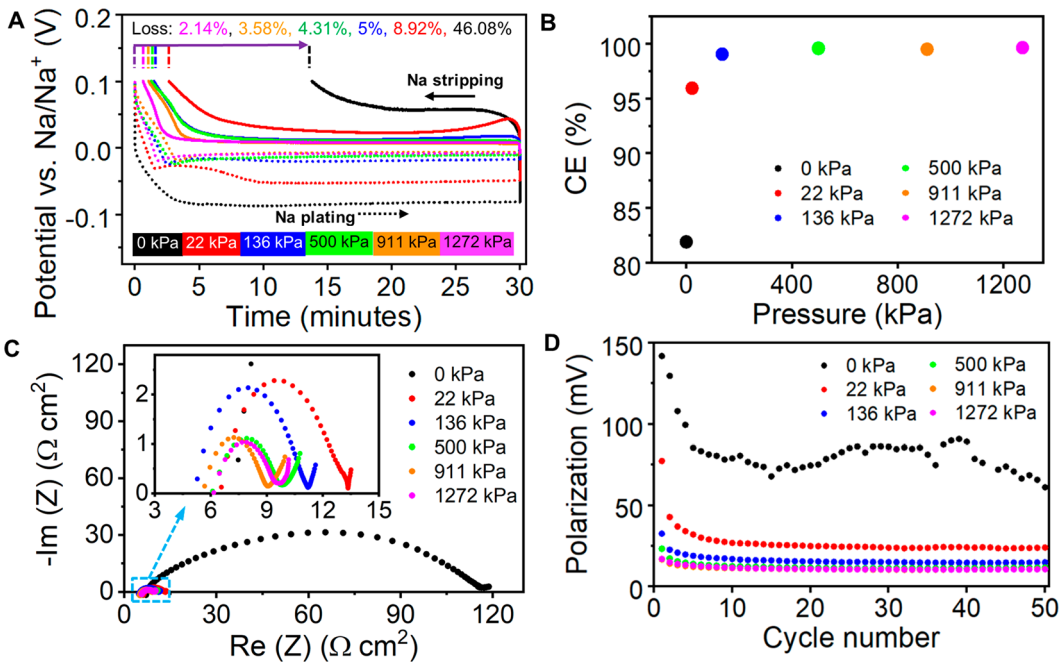

Figure 2. Electrochemical performance of the Na-C45 cell under various external pressures. (A) Slippage profiles for Na plating and stripping in the second cycle performed at 0.5 mA cm^{-2} under different pressures. (B) Average CE under different pressures performed at 0.5 mA cm^{-2} with a capacity of 0.25 mAh cm^{-2}. (C) Nyquist curves recorded under different pressures after the second deposition cycle. (D) Voltage polarization under various pressures.

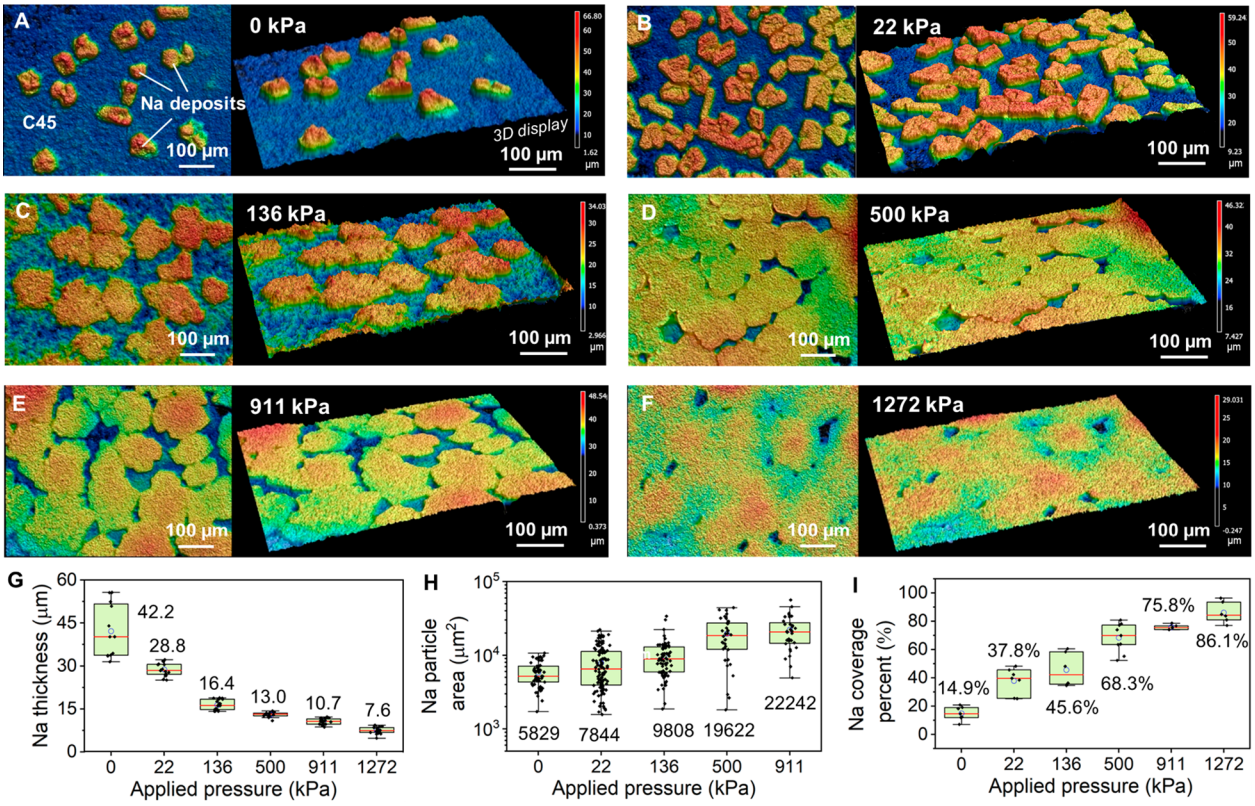

Figure 3. Growth patterns and physical features of Na after the second deposition cycle under various pressures. (A−F) Top and 3D views of Na deposited under (A) 0 kPa, (B) 22 kPa, (C) 136 kPa, (D) 500 kPa, (E) 911 kPa, and (F) 1272 kPa at 0.5 mA cm^{-2} for 0.5 h. (G−I) The corresponding thicknesses (G), individual areas (H), and area coverage fractions on the C45 layer (I) of Na deposition under various pressures obtained from CSLM test.

tests (Figure S3) at 0.5 mA cm^{-2} and subsequent imaging of the Na morphology via CLSM and scanning electron microscopy (SEM). To benchmark pressure effects on the Na battery system, we assembled coin cells of the same

https://doi.org/10.1021/acsenergylett.3c00734
ACS Energy Lett. 2023, 8, 2711−2717

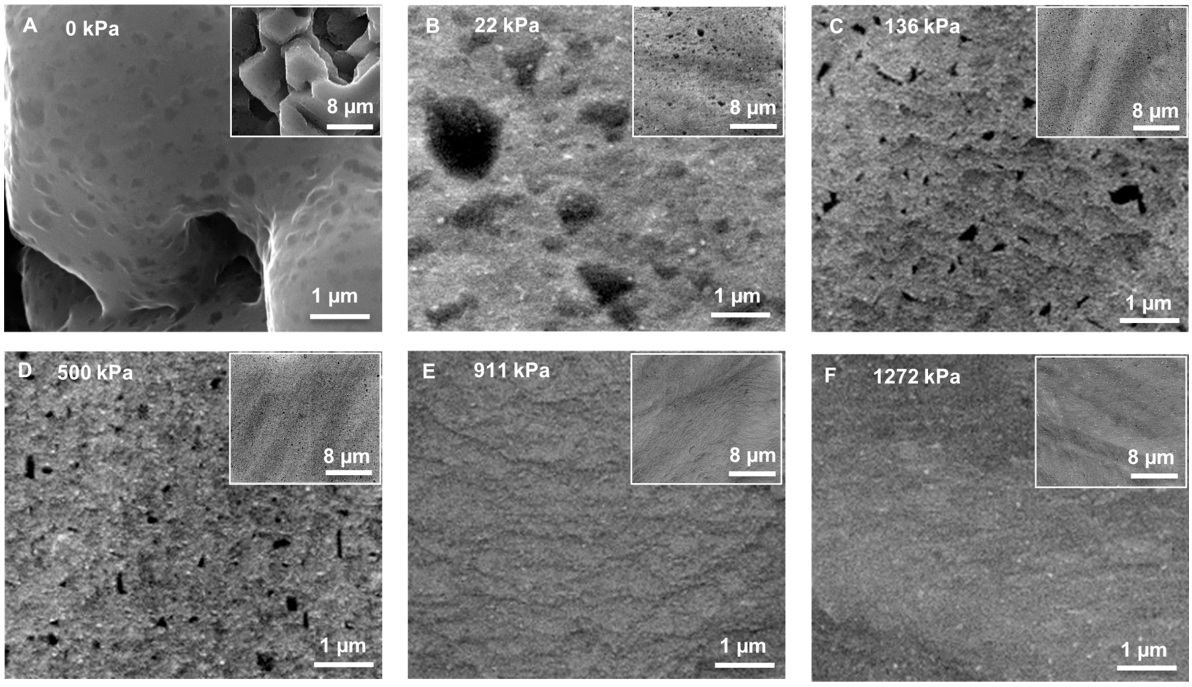

Figure 4. SEM images of Na deposition under various pressures after the second plating cycle at 0.5 mA cm^{-2} to a capacity of 0.25 mAh cm^{-2}. (A−F) Surface morphology of Na deposited under (A) 0 kPa, (B) 22 kPa, (C) 136 kPa, (D) 500 kPa, (E) 911 kPa, and (F) 1272 kPa. The insets show the respective lower magnification SEM images.

electrode materials as used in our pressure cell and observed a high average CE of 99.93% over a period of 1000 cycles (Figure S4), indicating performance competitive with that of leading state-of-the-art systems in recent literature.[27−30] However, to understand and distinguish the role of pressure, especially in the early stages of formation, we carried out galvanostatic cycling at different pressures for 50 cycles, which leads to a slightly lower overall average CE due to the influence of the first several cycles. Figure 2A shows the plating−stripping curves of the second cycle for each pressure condition studied, using slip plots to visualize the losses (first cycle loss is visualized in Figure S17). Notably, the second cycle loss decreased from 46.08% at 0 kPa to only 2.04% at 1272 kPa, indicating improved stability. Figure 2B and Figure S5 shows the CE for each cycle and average CE for each pressure over the period of 50 cycles studied, indicating an evident correlation. The average CE values at 0, 22, 136, and 500 kPa were 81.89%, 95.94%, 99.05%, and 99.59%, respectively, over 50 cycles, emphasizing that the largest Na metal losses occurred in the first 50 cycles at the lowest pressures. At pressures greater than 500 kPa, there were only slight increases in the CE over a 50-cycle duration.

Further, to better understand this influence of pressure, electrochemical impedance spectroscopy (EIS) was carried out. At the open-circuit voltage (OCV) prior to Na electroplating (Figure S6), the charge-transfer resistance (R_{ct}) is similar for all pressures except for the highest pressure (1272 kPa), where R_{ct} is slightly lower. However, EIS analysis after the second Na plating cycle (Figure 2C) indicates much different characteristics, where the value of R_{ct} significantly decreases based on the pressure applied to the cell. The cell at 0 kPa displays higher R_{ct} (∼110 Ω cm^2) than cells under pressure, and there is little effect on the value of R_{ct} after the pressure is increased beyond ∼500 kPa (a range of 3.4−3.7 Ω cm^2). These observations indicate there is no effect of pressure on performance in open-circuit conditions before Na is electroplated, but then it evolves in tandem with Na metal electrodeposition. To better elucidate this, the voltage polarization under different applied pressures was studied (Figure 2D), which quantifies the difference between the equilibrium plating and stripping potentials for Na (Figure S7). Similar to pressure effects on the CE, the average voltage polarization decreased when the pressure increased until near 500 kPa, with minimal changes at higher pressures.

Collectively, the electrochemical results in Figure 2 indicate that both charge loss and charge-transfer resistance are reduced when pressure is increased. Whereas pressure effects have been observed in Li metal cells,[22,31,32] the effects observed for Na metal cells here are notably at lower and more practical pressures (near 0.5 kPa) where damage to the separator does not influence transport. Our findings support that these EIS results could be explained by the changing properties of the Na at higher pressures versus lower pressures. At low pressures (<500 kPa), the low CE leads to greater accumulation of insulating side products and dead Na that likely contribute toward higher overall charge-transfer resistance at the Na−electrolyte interface. To better understand this observation and the mechanism driving these pressure-induced differences, we carried out studies of electrodeposited Na morphology using both CLSM (Figure 3) and SEM (Figure 4).

To perform morphological characterization of Na deposits, we first utilized CLSM in an airtight optical cell (Figure S8) to study the microscale morphology of Na deposits on C45 nucleation layers at different pressures (Figure 3A−F). CLSM is a noncontact analysis technique that provides micron-scale resolution in the x−y plane parallel to the current collector, and nanometer scale resolution in the z (height) plane. Notably, from pressures of 0 to 500 kPa, the morphology of Na deposits undergoes a drastic transition, from 3D nuclei structures at low pressures to smooth and homogeneous

https://doi.org/10.1021/acsenergylett.3c00734
ACS Energy Lett. 2023, 8, 2711−2717

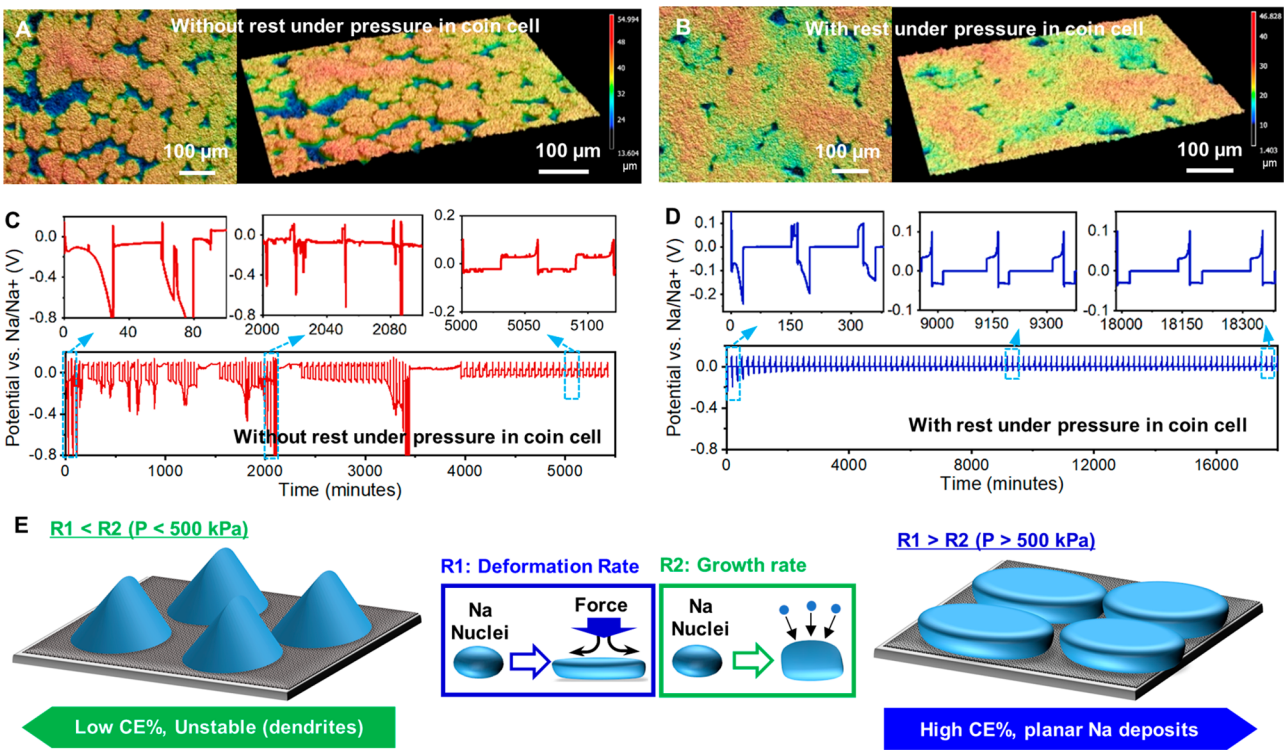

Figure 5. Effect of pressure-driven creep on Na deposits. CSLM images of Na deposits (A) without rest and (B) with rest under standard coin cell pressure. Galvanostatic cycling performance at 5 mA cm^{-2} (C) without rest and (D) with 2 h rest under pressure in coin cells with enlarged voltage profiles. (E) Schematic of the interplay between the Na deposition rate and the rate of mechanical deformation and morphology evolution of Na metal deposits observed in this study.

planar deposits near and above 500 kPa. At pressures higher than 500 kPa, the overall morphology of the deposits does not significantly change, but the deposits are more interconnected at higher pressures. To quantify the effect of pressure on the properties of Na deposits, several representative CLSM images at different pressures were subjected to laser measurement and image processing methods (ImageJ[33]) were used to identify geometrical characteristics, including (1) the average thickness of Na deposits (Figure 3G, by laser on CLSM), (2) the average area of Na deposits (Figure 3H, by ImageJ), and (3) the fractional area of Na on the current collector (Figure 3I, by ImageJ). In each case, results are presented in a statistical dot-plot representation to establish how each geometrical feature changes as a function of pressure.

As shown in Figure 3G, the average Na deposit thickness at 0 kPa is ∼42.2 μm (with significant height variation), which decreases to ∼7.6 μm at 1272 kPa in a compact range of values. A similar observation is made for the average individual Na deposit area, as the average deposit scales from ∼5829 μm^2 to ∼22242 μm^2 from 0 to 911 kPa (Figure 3H). Due to the interconnected nature of Na deposits at 1272 kPa, the total coverage was also analyzed (Figure 3I), and it was shown that the coverage fraction of Na improves from 14.9% at 0 kPa to 86.1% at 1272 kPa.

While CLSM is a valuable tool to visualize the morphology changes of Na at different pressures, it does not have the resolution to assess the microstructure of the Na, such as the porosity. However, comparing the analyses of CLSM images to calculations of fully dense Na at a capacity of 0.25 mAh cm^{-2}, the theoretical thickness of the Na at 86% coverage should be 2.5 μm, which is lower than that observed by imaging. This suggests that the microstructure and porosity of the Na deposits could also be changing at different pressures. To evaluate this point, SEM analysis was carried out (Figure 4) using a sealed Ar transfer cell that prevents air exposure during transfer between the glovebox and the SEM instrument. At 0 kPa (Figure 4A), porosity in the Na deposits exist at both the microscale and nanoscale, as is expected in 3D deposits. However, as the pressure is increased to and above 500 kPa, the pores in the Na deposits become smaller and are too small to resolve at pressures of 911 kPa and above. This supports that the effect of pressure on morphology is manifested both in microscale morphology (e.g., 2D versus 3D deposits) as well as in the nanoscale porosity of the Na layers.

In considering the results presented this far, it is clear that increasing pressure leads to thinner, more uniform, and less porous (denser) Na deposits, especially at pressures near and above 500 kPa (Figure 3, Figure 4). At pressures where 3D Na deposits are observed (<500 kPa), the electrochemical features indicate poorer charge reversibility and greater interfacial resistances for charge transfer (Figure 2C). This opens a key question as to whether the Na morphology is a result of planar growth from Na nuclei (the morphology is static and unchanging except for growth) or the morphology is changing dynamically due to pressure applied in the system. Prior modeling studies have shown that pressure can influence the static shape profile of 3D dendritic Li metal structures[23] and dynamic effects such as creep are not feasible at pressures near and below 1 MPa for Li.[25] However, the mechanical properties of Na are significantly different from those of Li—the stress exponent for Na is 5 versus 6.56 for Li, indicating a much greater influence of creep for Na metal.[18−20] Furthermore, the effective hardness of Na is 15 MPa versus 48 MPa for Li.[25,34] Recent results have shown that, at solid−solid interfaces at 1

https://doi.org/10.1021/acsenergylett.3c00734
ACS Energy Lett. 2023, 8, 2711−2717

MPa pressures, creep effects can modify the Na metal interface properties.[25] To evaluate the static versus dynamic responses of Na deposits to pressure (Figure 5), we carried out a study in a coin cell configuration (~1 MPa, Figure S9) at 10× higher plating/stripping current of 5 mA cm^{-2}. This higher current is utilized due to rate tests that indicate this is the current at which shorting effects occur under normal cycling (Figure S10 and Figure 5C).

To evaluate the dynamic behavior of the electroplated Na under pressure, we compared electrochemical and morphological characteristics of Na deposits after plating both with and without a 2 h rest stage (Figure S11). In this experiment, a rest step of 2 h is chosen as it allows the electrodeposited Na to reach a state of mechanical equilibrium under pressure, similar to the rationale of rest steps to reach electrochemical equilibrium in Galvanostatic Intermittent Titration Technique experiments. As shown in Figure 5 and illustrated in Figure S12, the morphology and electrochemical characteristics of the Na deposits are highly susceptible to dynamic changes and morphology evolution during this rest step. CLSM images of Na deposits without rest and with rest under pressure (Figure 5A,B) show a more interconnected, thinner (by over 25%, Figure S13), and planar film after undergoing a 2 h rest compared to electrodeposited Na imaged with no subsequent rest stage. SEM images in Figure S14 highlight a smoother and denser morphology of Na deposits after a 2 h rest.

Finally, 100 plating/stripping cycles using 30 min plating time at 5 mA cm^{-2} were conducted without rest and with a 2 h rest between plating/stripping steps (Figure 5C,D). Without rest, the voltage profiles exhibit soft-short behavior, likely due to dendrite or 3D Na formation at these high currents, but the devices exposed to 2 h rest at the same rate after electroplating showed a stable response with CE of 99.7% after 100 cycles (Figure S15). These findings indicate that the electrochemical stability of Na metal deposits at pressure conditions of standard coin and pouch cell packaging is dependent upon the interplay between morphological evolution and creep of the electrodeposited Na metal and the rate at which the Na metal is electrodeposited (i.e., the current density) in the experiments. Building from our findings, this interplay is visualized in Figure 5E, where under conditions of low morphological evolution or creep, such as at low pressures, the Na deposits exhibit 3D architectures and dendrite formation. However, at higher pressures >500 kPa, the influence of creep and/or morphological evolution of the Na leads to smooth layers with stable and efficient electrochemical behavior. Notably, these findings suggest that 3D morphologies and shorting effects can still occur under higher packaging pressures if the rate of Na electrodeposition is faster than the rate at which mechanical equilibrium is reached by morphology evolution and/or creep of Na metal. In turn, strategies to mitigate shorting effects and safety concerns for Na batteries may be more straightforward in Na metal batteries compared to Li batteries by leveraging the mechanical properties of Na at standard packaging pressures.

In summary, our findings give insight into the coupled chemo-mechanical behavior that is responsible for the stable, high performance of Na metal batteries widely reported in the literature. Our results indicate that dynamic creep and morphology evolution of electrodeposited Na at pressures relevant to coin and pouch cell packaging (500 kPa to 1.2 MPa) are responsible for the smooth Na deposits correlated to high Na metal Coulombic efficiency. These results support a picture different from that of Li metal batteries in that the mechanical equilibrium of the Na metal deposits is of equal or greater importance than electrochemical equilibrium for rate performance and/or safety outcomes. Further, we hypothesize from this work that pressure-induced deformation of Na and/or the nucleation layer, and more broadly a deeper understanding of chemo-mechanical coupling in this system, is more important toward achieving smooth, stable Na deposits compared to the widely held viewpoint of controlling and steering Na metal nucleation.

■ ASSOCIATED CONTENT

Supporting Information

The Supporting Information is available free of charge at https://pubs.acs.org/doi/10.1021/acsenergylett.3c00734.

Detailed experiment methods, additional SEM images, supplementary plating/stripping voltage profiles, schematics of pressure cell, coin cell, and airtight optical cell, and plots of CE versus cycle number for high current devices with and without rest periods (PDF)

■ AUTHOR INFORMATION

Corresponding Author

Cary L. Pint − *Department of Mechanical Engineering, Iowa State University, Ames, Iowa 50011, United States;* orcid.org/0000-0003-4700-0852; Email: carypint@iastate.edu

Authors

Weimin Jiao − *Department of Mechanical Engineering, Iowa State University, Ames, Iowa 50011, United States*

Murtaza Zohair − *Department of Mechanical Engineering, Iowa State University, Ames, Iowa 50011, United States*

Janna Eaves-Rathert − *Department of Mechanical Engineering, Vanderbilt University, Nashville, Tennessee 37235, United States*

Jayanth Ramamurthy − *Department of Mechanical Engineering, Iowa State University, Ames, Iowa 50011, United States*

Andrew Harkaway − *Department of Mechanical Engineering, Iowa State University, Ames, Iowa 50011, United States*

Rebecca Mort − *Department of Materials Science and Engineering, Iowa State University, Ames, Iowa 50011, United States*

Jacob Wheaton − *Department of Materials Science and Engineering, Iowa State University, Ames, Iowa 50011, United States;* orcid.org/0000-0001-8461-9393

Shan Jiang − *Department of Materials Science and Engineering, Iowa State University, Ames, Iowa 50011, United States;* orcid.org/0000-0001-8119-9012

Steve W. Martin − *Department of Materials Science and Engineering, Iowa State University, Ames, Iowa 50011, United States;* orcid.org/0000-0002-6472-509X

Complete contact information is available at: https://pubs.acs.org/10.1021/acsenergylett.3c00734

Notes

The authors declare no competing financial interest.

■ ACKNOWLEDGMENTS

The authors acknowledge Dr. Jaime Juarez for assistance with optical microscopy related to this study. This work was in part

supported by the State of Iowa, Iowa Energy Center, through grants IEC 024881 (C.L.P) and IEC 307352 (S.W.M.), the National Science Foundation (NSF) through grant DMR 1936913, and the Iowa Space Grant Consortium under NASA Award No. 80NSSC20M0107.

■ REFERENCES

(1) Seh, Z. W.; Sun, J.; Sun, Y.; Cui, Y. A Highly Reversible Room-Temperature Sodium Metal Anode. *ACS Cent. Sci.* **2015**, *1*, 449−455.

(2) Sun, B.; Xiong, P.; Maitra, U.; Langsdorf, D.; Yan, K.; Wang, C.; Janek, J.; Schröder, D.; Wang, G. Design Strategies to Enable the Efficient Use of Sodium Metal Anodes in High-Energy Batteries. *Adv. Mater.* **2020**, *32*, 1903891.

(3) Zhao, Y.; Adair, K. R.; Sun, X. Recent developments and insights into the understanding of Na metal anodes for Na-metal batteries. *Energy Environ. Sci.* **2018**, *11*, 2673−2695.

(4) Cohn, A. P.; Muralidharan, N.; Carter, R.; Share, K.; Pint, C. L. Anode-Free Sodium Battery through in Situ Plating of Sodium Metal. *Nano Lett.* **2017**, *17*, 1296−1301.

(5) Li, Y.; Zhou, Q.; Weng, S.; Ding, F.; Qi, X.; Lu, J.; Li, Y.; Zhang, X.; Rong, X.; Lu, Y.; Wang, X.; Xiao, R.; Li, H.; Huang, X.; Chen, L.; Hu, Y.-S. Interfacial engineering to achieve an energy density of over 200 Wh kg-1 in sodium batteries. *Nat. Energy* **2022**, *7*, 511−519.

(6) Hartmann, P.; Bender, C. L.; Vračar, M.; Dürr, A. K.; Garsuch, A.; Janek, J.; Adelhelm, P. A rechargeable room-temperature sodium superoxide (NaO2) battery. *Nat. Mater.* **2013**, *12*, 228−232.

(7) Reeve, Z. E. M.; Franko, C. J.; Harris, K. J.; Yadegari, H.; Sun, X.; Goward, G. R. Detection of Electrochemical Reaction Products from the Sodium-Oxygen Cell with Solid-State 23Na NMR Spectroscopy. *J. Am. Chem. Soc.* **2017**, *139*, 595−598.

(8) Xia, C.; Fernandes, R.; Cho, F. H.; Sudhakar, N.; Buonacorsi, B.; Walker, S.; Xu, M.; Baugh, J.; Nazar, L. F. Direct Evidence of Solution-Mediated Superoxide Transport and Organic Radical Formation in Sodium-Oxygen Batteries. *J. Am. Chem. Soc.* **2016**, *138*, 11219−11226.

(9) Wang, Y.-X.; Yang, J.; Lai, W.; Chou, S.-L.; Gu, Q.-F.; Liu, H. K.; Zhao, D.; Dou, S. X. Achieving High-Performance Room-Temperature Sodium-Sulfur Batteries With S@Interconnected Mesoporous Carbon Hollow Nanospheres. *J. Am. Chem. Soc.* **2016**, *138*, 16576−16579.

(10) Wei, S.; Xu, S.; Agrawral, A.; Choudhury, S.; Lu, Y.; Tu, Z.; Ma, L.; Archer, L. A. A stable room-temperature sodium-sulfur battery. *Nat. Commun.* **2016**, *7*, 11722.

(11) Xin, S.; Yin, Y.-X.; Guo, Y.-G.; Wan, L.-J. A High-Energy Room-Temperature Sodium-Sulfur Battery. *Adv. Mater.* **2014**, *26*, 1261−1265.

(12) Wang, H.; Matios, E.; Luo, J.; Li, W. Combining theories and experiments to understand the sodium nucleation behavior towards safe sodium metal batteries. *Chem. Soc. Rev.* **2020**, *49*, 3783−3805.

(13) Lee, B.; Paek, E.; Mitlin, D.; Lee, S. W. Sodium Metal Anodes: Emerging Solutions to Dendrite Growth. *Chem. Rev.* **2019**, *119*, 5416−5460.

(14) Peters, J.; Buchholz, D.; Passerini, S.; Weil, M. Life cycle assessment of sodium-ion batteries. *Energy Environ. Sci.* **2016**, *9*, 1744−1751.

(15) Yui, Y.; Hayashi, M.; Nakamura, J. In situ Microscopic Observation of Sodium Deposition/Dissolution on Sodium Electrode. *Sci. Rep.* **2016**, *6*, 22406.

(16) Ma, B.; Lee, Y.; Bai, P. Dynamic Interfacial Stability Confirmed by Microscopic Optical Operando Experiments Enables High-Retention-Rate Anode-Free Na Metal Full Cells. *Adv. Sci.* **2021**, *8*, 2005006.

(17) Cohn, A. P.; Metke, T.; Donohue, J.; Muralidharan, N.; Share, K.; Pint, C. L. Rethinking sodium-ion anodes as nucleation layers for anode-free batteries. *J. Mater. Chem. A* **2018**, *6*, 23875−23884.

(18) Masias, A.; Felten, N.; Garcia-Mendez, R.; Wolfenstine, J.; Sakamoto, J. Elastic, plastic, and creep mechanical properties of lithium metal. J. *J. Mater. Sci.* **2019**, *54*, 2585−2600.

(19) Wang, M. J.; Chang, J.-Y.; Wolfenstine, J. B.; Sakamoto, J. Analysis of elastic, plastic, and creep properties of sodium metal and implications for solid-state batteries. *Materialia* **2020**, *12*, 100792.

(20) Fincher, C. D.; Zhang, Y.; Pharr, G. M.; Pharr, M. Elastic and Plastic Characteristics of Sodium Metal. *ACS Appl. Energy Mater.* **2020**, *3*, 1759−1767.

(21) LePage, W. S.; Chen, Y.; Poli, A.; Thouless, M. D.; Dasgupta, N. P. Sodium mechanics: effects of temperature, strain rate, and grain rotation and implications for sodium metal batteries. *Extreme Mech. Lett.* **2022**, *52*, 101644.

(22) Yin, X.; Tang, W.; Jung, I. D.; Phua, K. C.; Adams, S.; Lee, S. W.; Zheng, G. W. Insights into morphological evolution and cycling behaviour of lithium metal anode under mechanical pressure. *Nano Energy* **2018**, *50*, 659−664.

(23) Shen, X.; Zhang, R.; Shi, P.; Chen, X.; Zhang, Q. How Does External Pressure Shape Li Dendrites in Li Metal Batteries? *Adv. Energy Mater.* **2021**, *11*, 2003416.

(24) Fang, C.; Lu, B.; Pawar, G.; Zhang, M.; Cheng, D.; Chen, S.; Ceja, M.; Doux, J.-M.; Musrock, H.; Cai, M.; Liaw, B.; Meng, Y. S. Pressure-tailored lithium deposition and dissolution in lithium metal batteries. *Nat. Energy* **2021**, *6*, 987−994.

(25) Zhang, X.; Wang, Q. J.; Peng, B.; Wu, Y. Pressure-Driven and Creep-Enabled Interface Evolution in Sodium Metal Batteries. *ACS Appl. Mater. Interfaces* **2021**, *13*, 26533−26541.

(26) Spencer Jolly, D.; Ning, Z.; Darnbrough, J. E.; Kasemchainan, J.; Hartley, G. O.; Adamson, P.; Armstrong, D. E. J.; Marrow, J.; Bruce, P. G. Sodium/Na β'' Alumina Interface: Effect of Pressure on Voids. *ACS Appl. Mater. Interfaces* **2020**, *12*, 678−685.

(27) Park, S.; Jin, H.-J.; Yun, Y. S. Effects of Carbon-Based Electrode Materials for Excess Sodium Metal Anode Engineered Rechargeable Sodium Batteries. *ACS Sustain Chem. Eng.* **2020**, *8*, 17697−17706.

(28) Li, T.; Sun, J.; Gao, S.; Xiao, B.; Cheng, J.; Zhou, Y.; Sun, X.; Jiang, F.; Yan, Z.; Xiong, S. Superior Sodium Metal Anodes Enabled by Sodiophilic Carbonized Coconut Framework with 3D Tubular Structure. *Adv. Energy Mater.* **2021**, *11*, 2003699.

(29) Wang, Y.; Dong, H.; Katyal, N.; Hao, H.; Liu, P.; Celio, H.; Henkelman, G.; Watt, J.; Mitlin, D. A Sodium-Antimony-Telluride Intermetallic Allows Sodium-Metal Cycling at 100% Depth of Discharge and as an Anode-Free Metal Battery. *Adv. Mater.* **2022**, *34*, 2106005.

(30) Lee, K.; Lee, Y. J.; Lee, M. J.; Han, J.; Lim, J.; Ryu, K.; Yoon, H.; Kim, B.-H.; Kim, B. J.; Lee, S. W. A 3D Hierarchical Host with Enhanced Sodiophilicity Enabling Anode-Free Sodium-Metal Batteries. *Adv. Mater.* **2022**, *34*, 2109767.

(31) Harrison, K. L.; Goriparti, S.; Merrill, L. C.; Long, D. M.; Warren, B.; Roberts, S. A.; Perdue, B. R.; Casias, Z.; Cuillier, P.; Boyce, B. L.; Jungjohann, K. L. Effects of Applied Interfacial Pressure on Li-Metal Cycling Performance and Morphology in 4 M LiFSI in DME. *ACS Appl. Mater. Interfaces* **2021**, *13*, 31668−31679.

(32) Qin, L.; Wang, K.; Xu, H.; Zhou, M.; Yu, G.; Liu, C.; Sun, Z.; Chen, J. The role of mechanical pressure on dendritic surface toward stable lithium metal anode. *Nano Energy* **2020**, *77*, 105098.

(33) Schneider, C. A.; Rasband, W. S.; Eliceiri, K. W. NIH Image to ImageJ: 25 years of image analysis. *Nat. Meth.* **2012**, *9*, 671−675.

(34) Zhang, X.; Wang, Q. J.; Harrison, K. L.; Roberts, S. A.; Harris, S. J. Pressure-Driven Interface Evolution in Solid-State Lithium Metal Batteries. *Cell Rep. Phys. Sci.* **2020**, *1*, 100012.